

University of Nebraska - Lincoln
DigitalCommons@University of Nebraska - Lincoln

NASA Publications

National Aeronautics and Space Administration

2012

Atmospheric correction for MASTER image data using localized modelled and observed meteorology and trace gases

Daniel S. Tkacik
Carnegie Mellon University

Yaítza Luna-Cruz
Howard University

Nicholas Clinton
Airborne Sensor Facility, NASA Ames Research Center, Moffett Field, CA, nicholas.clinton@nasa.gov

Scott Spak
University of Iowa

John Ryan
Monterey Bay Aquarium Research Institute, Moss Landing, CA

Follow this and additional works at: <http://digitalcommons.unl.edu/nasapub>

Tkacik, Daniel S.; Luna-Cruz, Yaítza; Clinton, Nicholas; Spak, Scott; and Ryan, John, "Atmospheric correction for MASTER image data using localized modelled and observed meteorology and trace gases" (2012). *NASA Publications*. 199.
<http://digitalcommons.unl.edu/nasapub/199>

This Article is brought to you for free and open access by the National Aeronautics and Space Administration at DigitalCommons@University of Nebraska - Lincoln. It has been accepted for inclusion in NASA Publications by an authorized administrator of DigitalCommons@University of Nebraska - Lincoln.

Atmospheric correction for MASTER image data using localized modelled and observed meteorology and trace gases

DANIEL S. TKACIK†, YAÍTZA LUNA-CRUZ‡, NICHOLAS CLINTON*§,
SCOTT SPAK¶ and JOHN RYAN|

†Department of Civil and Environmental Engineering, Carnegie Mellon University,
Pittsburgh, PA, USA

‡NOAA Center for Atmospheric Sciences, Howard University, Washington, DC, USA

§Airborne Sensor Facility, NASA Ames Research Center, Moffett Field, CA, USA

¶Center for Global and Regional Environmental Research, University of Iowa, Iowa
City, IA, USA

|Monterey Bay Aquarium Research Institute, Moss Landing, CA, USA

(Received 23 August 2010; in final form 24 December 2010)

Atmospheric correction for remote sensing-based studies typically does not use information from spatio-temporally resolved meteorological models. We assessed the effect of using observations and mesoscale weather and chemical transport models on multispectral retrievals of land and ocean properties. We performed two atmospheric corrections on image data acquired by the Moderate Resolution Imaging Spectroradiometer (MODIS)/Advanced Spaceborne Thermal Emission and Reflection Radiometer (ASTER) airborne simulator over Monterey Bay, California. One correction used local atmospheric profiles of meteorology and trace gases at overpass and the other used the 1976 US Standard default atmospheric profile in the MODTRAN4 radiative transfer model. We found only minor impacts from atmospheric correction in the Fluorescence Line Height index of ocean chlorophyll, but substantive differences in retrievals of surface temperature and the Normalized Difference Vegetation Index. Improvements in sea surface temperature retrieval were validated by *in situ* measurements. Results indicate that spatio-temporally specific atmospheric correction factors from mesoscale models can improve retrievals of surface properties from remotely sensed image data.

1. Introduction

The signal detected by a remote sensor is the overall result of three main radiative contributions: direct reflection from the target, scattering from the atmosphere and reflected radiation (from the target and elsewhere) diffusely transmitted to the sensor (Verhoef and Bach 2003). The radiance measured from land and ocean ecosystems at the Earth's surface may be biased by the radiance of atmospheric constituents located between the surface and the sensor (Adler-Golden *et al.* 1999). Correcting for these biases is crucial in accurately characterizing various surface-level phenomena using remote sensing techniques. To address this problem, a comparison of the MODerate

*Corresponding author. Email: nicholas.clinton@nasa.gov

Spectral resolution atmospheric TRANSMittance algorithm and Computer Model (MODTRAN4)-based atmospheric correction methods is presented and evaluated in this study.

Atmospheric correction has been shown to increase classification accuracy of remotely sensed image data (Huang *et al.* 2008). Letelier and Abbott (1996) discussed how atmospheric correction affects ocean chlorophyll indices. Other studies address the effect of atmospheric correction on the Normalized Difference Vegetation Index (NDVI) (Tanre *et al.* 1992, Vermote *et al.* 1997). In light of these sensitivity analyses, generic atmospheric correction methods have become *de rigueur* for many remote sensing studies in which atmospheric effects are a concern. Monthly and seasonal profiles from global atmospheric chemical transport models have been used to correct column retrievals of trace gases (e.g. Palmer *et al.* 2001, Martin 2002, Lee *et al.* 2009), although this has yet to be implemented in operational retrievals. However, instantaneous output from mesoscale atmospheric models is not commonly used to inform the radiative transfer calculations used for atmospheric correction in remotely sensed image data. In this case study, we quantify the differences in land and ocean surface properties resulting from atmospheric correction derived from default or incomplete assumed vertical profiles and correction derived from a suite of local, spatio-temporally specific atmospheric constituents.

2. Data and methods

2.1 Study site and remote sensing data

A DC-8 research aircraft, owned and operated by the National Aeronautics and Space Administration (NASA) and the National Suborbital Education and Research Center (NSERC), was flown over the Monterey Bay region on 22 July 2009 starting at 23:48:43 and ending at 23:53:31 UTC, as part of the NASA/NSERC Student Airborne Research Program. The aircraft heading was specified to be as close to solar azimuth as possible to minimize illumination effects in the image data. Aboard the DC-8, the Moderate Resolution Imaging Spectroradiometer (MODIS)/Advanced Spaceborne Thermal Emission and Reflection Radiometer (ASTER) airborne simulator (MASTER) (Hook *et al.* 2001) acquired image data over Monterey Bay from an altitude of 11 207 m, for a pixel size of 17.7 m. MASTER collects image data in 50 spectral bands in a range from 0.44 to 13 μm (Hook *et al.* 2001). Image data were processed to at-sensor radiance prior to application of the atmospheric correction. A supervised classification of at-sensor radiance was used to identify three land-cover categories in the study area: photosynthetically active vegetation, dry grass/urban/unvegetated areas and ocean. The categories were identified based on spectral angle similarity to hand delineated training areas.

2.2 Modelled atmospheric profile

There are no routine observations of atmospheric profiles near the study site, so simulated profiles from weather and atmospheric chemistry forecast models were used to estimate the instantaneous profiles of meteorology and trace gases over Monterey Bay during the MASTER overpass. An 18-layer atmospheric profile of pressure, temperature, dew point temperature and wind speed over the study domain from the surface to the aircraft altitude at 0 UTC on 23 July was extracted from a hemispheric simulation with the Advanced Research Weather Research and Forecasting (WRF) model version 2.2 (Skamarock *et al.* 2005) at 50 km horizontal resolution. The Sulphur Transport Eulerian Model (STEM)-2K3 chemical transport model (Carmichael *et al.* 2003),

configured as in Adhikary *et al.* (2010) with the Statewide Air Pollution Research Center (SAPRC)99 gas-phase chemical mechanism (Carter 1999) and driven by WRF meteorology, simulated chemical transport over the region in support of research flight planning. Simulated vertical profiles of STEM ozone, carbon monoxide, nitrogen oxide, nitrogen dioxide, sulphur dioxide, ammonia and gaseous nitric acid were taken from the grid cell covering the study domain. Trace gas concentrations for long-lived, well-mixed species not included in the STEM simulation, including nitrous oxide, carbon dioxide and methane, were updated with contemporaneous daily surface observations at the National Oceanic and Atmospheric Administration (NOAA) Earth Systems Research Laboratory Global Monitoring Division Trinidad Head Observatory 660 km north along the California coast, the nearest location with routine measurements.

There are always numerous uncertainties in all aspects of this type of modelling system, namely emissions; initial conditions from the global forecast model; boundary and initial conditions for trace gases and aerosols; the meteorological model; the chemical transport model's (CTM) chemistry and physics; and the mesoscale models' horizontal, vertical and temporal resolution. In this case, the integrated forecasting system has been found to simulate the spatial and temporal features of observed aircraft and surface summertime meteorology, ozone and speciated fine particle concentrations over California (Huang *et al.* 2010a, 2010b). The most important aspect of uncertainty in this application of modelled atmospheric profiles is that net uncertainties, biases and errors in the spatially and temporally specific modelled profiles for every component of the profile will always be smaller than the uncertainties in a default profile, and often by orders of magnitude.

2.3 Radiative transfer modelling

The MODerate spectral resolution atmospheric TRANsmittance algorithm and computer model (MODTRAN4) (Berk *et al.* 1999) was used to model the spectral absorption, transmission, emission and scattering characteristics of the atmosphere. MODTRAN4 was run with its default atmospheric profile (hereafter referred to as DG for default gas settings) in which only pressure, temperature and humidity were specified for the 18 atmosphere layers. For the WRF/STEM/observed profile (IG for input gas), the trace gases described in section 2.2 were entered at the 18 layers. In both settings, based on low simulated aerosol concentrations and low MODIS aerosol optical depth retrievals over the study area, the default aerosol attenuation of maritime extinction with 23 km visibility (MODTRAN4 default) was used in conjunction with the Navy Oceanic Vertical Aerosol Model (NOVAM). Radiative transfer was simulated three times for each profile for a simulated Lambertian surface with spectrally flat surface albedos of 0.0, 0.5 and 1.0, which allowed for the estimation of ground reflectance for the central wavelength of each MASTER band (Verhoef and Bach 2003). Ground temperature was determined by first determining upwelling ground radiance, then inverting the Planck equation with an assumed emissivity of 0.98 (Schmugge *et al.* 2002).

2.4 Calculation of surface properties from output data

Image data produced from the IG and DG MODTRAN4 calculations were used to estimate two indices of surface-relevant properties. Fluorescence Line Height (FLH) (Letelier and Abbott 1996), which quantifies radiation emitted from the ocean surface in the chlorophyll fluorescence emission band, is defined as

$$FLH = \rho_6 - \left[\rho_7 + (\rho_5 - \rho_7) \left[\frac{(\lambda_7 - \lambda_6)}{(\lambda_7 - \lambda_5)} \right] \right] \quad (1)$$

where ρ is retrieved reflectance and λ is wavelength subscripted by MASTER band index.

NDVI (Huete *et al.* 2002), which is a radiative index of the photosynthetic capacity and energy absorption of plant canopies, is defined as

$$NDVI = \frac{\rho_7 - \rho_5}{\rho_7 + \rho_5} \quad (2)$$

Temperature images were produced using radiance data from MASTER band 43 (8.62 μm), which was found to correspond best with *in situ* data, measured at the time of overflight, from a shipboard sea surface thermometer.

2.5 Statistical comparison of MASTER-retrieved properties and *in situ* measurements

In situ measurements of sea-surface temperature and chlorophyll were collected by ship (see <http://marineops.mlml.calstate.edu/JM-SciEquip> for a description of this platform) in Monterey Bay during the time of the MASTER overpass. The ship-measured data were overlaid on the MASTER image data for the purpose of accuracy assessment. Mean error, mean bias, mean fractional error, mean fractional bias and root mean square error were computed for the temperature retrievals using DG settings and compared against the retrievals using the IG settings to assess any improvement or worsening of the retrievals' accuracy. As the units of *in situ* chlorophyll measurements differ from the units of chlorophyll indices derived from remotely sensed image data, we compare these data sets using the squared correlation coefficient (R^2).

3. Results

3.1 Transmittance

MODTRAN4 calculated individual transmittance data for all input gases as well as total transmittance. The total transmittance curves of the IG and DG runs are plotted side by side along with a difference in the two curves (figure 1).

3.2 *In situ* validation of temperature and FLH retrieval

In situ measurements of sea-surface temperature and chlorophyll were statistically analysed alongside the MASTER-retrieved temperature and FLH to validate a more accurate retrieval using the IG settings. The temperature results are summarized in table 1. Sea-surface temperatures retrieved using IG settings showed substantial improvement for all statistics considered. IG-derived FLH showed a negligible increase in R^2 (from 0.004 to 0.007), although the correlation in both cases is so close to zero, it is clear that the bio-optical signal in this scene is too low for detection through remote sensing.

3.3 Comparison of surface properties

FLH, NDVI and temperature images were produced for both default and modelled atmospheric profiles and compared by pixel-wise subtraction of the IG image data from the DG image data. Difference images corresponding to NDVI, temperature (in

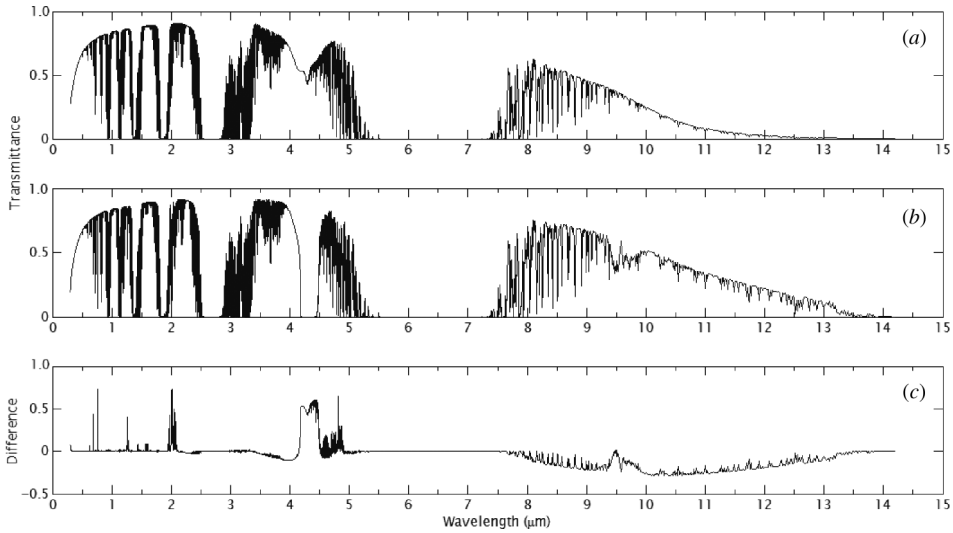


Figure 1. Transmittances using DG (default gas settings) and IG (input gas) profiles in MODTRAN4 ((a) and (b), respectively) and the difference between DG and IG, found by subtracting IG from DG (c).

Table 1. Mean error (ME), mean bias (MB), mean fractional error (MFE), mean fractional bias (MFB) and root mean square error (RMSE) computed for temperature in respect to *in situ* measurements, for both DG and IG settings.

	DG	IG
ME	2.1108	1.3304
MB	1.8686	1.0900
MFE	0.0073	0.0046
MFB	0.0064	0.0038
RMSE	3.0541	1.6546

kelvin) and FLH are shown in figure 2((a)–(c)), respectively. Figure 2((a)–(c)) contains non-georeferenced image data and is oriented to the in-flight direction rather than true north. This eliminates the need to perform a re-sampling of the pixel values. The images in figure 2((a)–(c)) were all stretched using a histogram equalization in order to enhance spatial patterns in the differences.

These comparisons are quantified in table 2 for each land-cover category. Table 2 reports the mean values from the DG image, the IG image, the difference (DG – IG) image and the root mean square (RMS) of the difference image. The RMS difference in temperature retrievals between the two gas-setting scenarios ranges from 0.981 to 6.786 (0.34–2.4% of the DG output). Differences in FLH are of the same magnitude as the FLH outputs in both scenarios, although the FLH retrievals themselves indicated nil to zero chlorophyll content. RMS difference in NDVI retrievals ranged from 0.024 to 0.091 (3.9–24.7% of DG output).

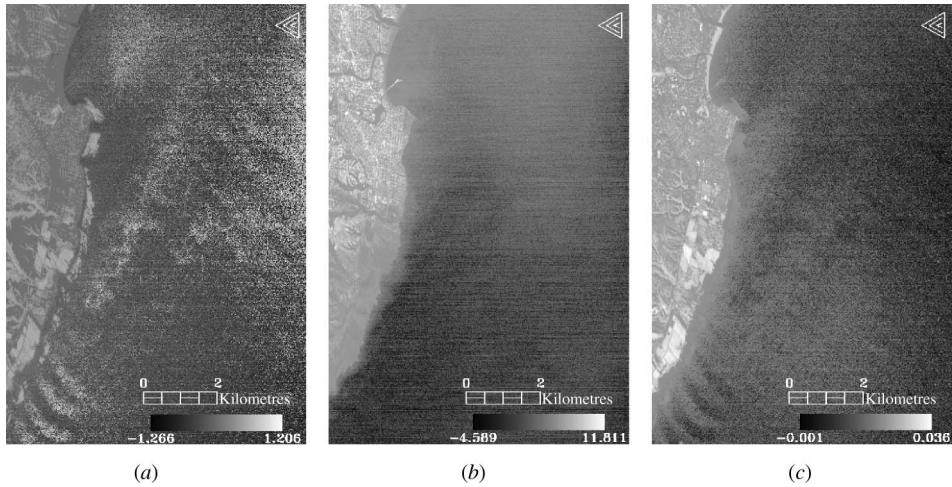


Figure 2. Difference images (DG – IG) containing forested areas on the left part of the image, the city of Santa Cruz, CA, USA, and portions of Monterey Bay on the right: (a) NDVI, (b) temperature, (c) FLH.

Table 2. Retrieved values for NDVI, T (K) and FLH scene averages for DG and IG atmospheric profiles, the mean difference (DG – IG) and the root mean square (RMS) differences for three land-cover categories.

		Ocean	Vegetation	Dry grass/urban
Temperature (K)	DG	286.808	306.776	316.721
	IG	286.914	302.244	310.133
	Mean difference	-0.106	4.532	6.588
	RMS difference	0.981	4.792	6.786
FLH	DG	0.001	-0.014	-0.006
	IG	-0.001	-0.023	-0.017
	Mean difference	0.002	0.008	0.011
	RMS difference	0.002	0.008	0.011
NDVI	DG	0.368	0.588	0.293
	IG	0.425	0.610	0.326
	Mean difference	-0.058	-0.022	-0.033
	RMS difference	0.091	0.023	0.034

4. Discussion

Figure 1 shows that the radiative properties retrieved with the two atmospheric corrections are substantially different. The largest differences are found between 4 and 5 μm , which are absorption bands for carbon dioxide, nitrous oxide and ozone. Here, the IG output is shown to be up to 50% different from the DG output. There are also a few positive spikes, notably around 2 μm , which represent a water vapour absorption band and a widespread area of difference across the 8–14 μm range due primarily to water vapour, with smaller isolated contributions from carbon dioxide, methane, nitrous oxide and ozone. Sub-micron differences in water vapour absorption impact the thermal range in the resulting retrieval, with the integrated effect from 8 to 14 μm in the IG profile leading to a net increase in transmittance across the modelled spectrum.

The results of the statistical analysis shown in table 1 indicate that temperatures derived using IG settings are in closer agreement with *in situ* data than temperatures derived using DG settings, which suggests an improvement in accuracy when using IG settings. The temperature difference image shown in figure 1 reveals visible differences in temperature between the IG and DG cases. When the numerical values are compared (table 2), the DG retrieves higher temperatures (indicated by positive values for DG minus IG) than the IG case, with larger differences over land. This could explain overestimation of surface temperature in some remote sensing retrievals of temperature. This is particularly important for studies investigating high temperature targets such as urban heat islands (e.g. Lo *et al.* 1997).

Although no available *in situ* measurements of NDVI were collected, the NDVI images produced show notable differences between the two gas settings (figure 2(a), table 2), which suggests that NDVI is highly sensitive to these settings. The IG case generally retrieves higher values for NDVI than the DG case, with RMS difference 0.023 (4%) over a vegetated landscape. Over a land-cover type (dry grass/urban) with lower NDVI, the RMS difference increases to 0.034 (11%). This finding suggests that in studies of re-vegetation and phenology change (e.g. Clinton *et al.* 2010), use of locally representative modelled atmospheric profiles could have an impact on detection of low level photosynthetic activity.

When *in situ* measurements were collected by ship, chlorophyll content was found to be negligible. This prevents any statistical claims from being made about the accuracy performance of DG versus IG FLH retrievals. In figure 2(c), the difference in FLH between the two cases is seen visibly, but all values yield the same qualitative result of low to nil chlorophyll content (table 1), with net RMS difference of 0.002 over the ocean. For the most part, the difference in the DG and IG chlorophyll content over Monterey Bay is negligible. However, near shore areas the difference in FLH is nearly twice as large as in the offshore areas where negligible chlorophyll was measured *in situ*, suggesting that the use of input gas profiles in atmospheric correction could affect detection of harmful algal bloom refugia (e.g. Ryan *et al.* 2008).

5. Conclusion

Two atmospheric cases were simulated using MODTRAN4 to determine the radiative interactions of the atmosphere with the land and ocean surface. One case employed the default MODTRAN4 atmospheric profile, whereas the other used meteorological and trace gas profiles extracted from a hemispheric chemical transport model. Retrieved MASTER NDVI, FLH and temperature all yielded numerically different results from air-mass correction using the two MODTRAN4 simulations. Temperature retrievals showed an improvement in accuracy, validated by *in situ* measurements. Temperature differences between the two gas settings may help explain the overestimation of temperature by remote sensors using default atmospheric profiles. Differences in NDVI values suggest that including locally specific atmospheric correction factors may improve the ability to distinguish areas of vegetation recovery and early phenological stages.

Overall, changes in image data are attributable predominantly to species whose atmospheric profiles are operationally retrieved, modelled or observed by routine radiosondes. The increasing global coverage of high-resolution operational forecast and reanalysis models for weather and atmospheric chemistry, along with a new generation of vertically resolved satellite retrievals of trace gases and aerosols, provide a wealth of data supporting further application of atmospheric correction to remotely

sensed image data. The impact of spatio-temporally specific atmospheric correction for retrieved MODIS and ASTER image data should be further assessed in the future on a global basis, and may merit inclusion in reanalyses and future operational retrieval algorithms.

Acknowledgements

This research was supported by the National Aeronautics and Space Administration (NASA) and the National Suborbital Education and Research Center (NSERC) during the 2009 Student Airborne Research Program (SARP). *In situ* data collection was supported by R. Kudela (University of California, Santa Cruz).

References

- ADHIKARY, B., CARMICHAEL, G.R., KULKARNI, S., WEI, C., TANG, Y. and ALLURA, A.D., 2010, A regional scale modeling analysis of aerosol and trace gas distributions over the eastern Pacific during the INTEX-B field campaign. *Atmospheric Chemistry and Physics*, **10**, pp. 2091–2115.
- ADLER-GOLDEN, S.M., MATTHEW, M.W., BERNSTEIN, L.S., LEVINE, R.Y., BERK, A., RICHTSMIEIER, S.C., ACHARYA, P.K., ANDERSON, G.P., FELDE, G., GARDNER, J., HOKE, M., JEONG, L.S., PUKALL, B. and MELLO, J., 1999, Atmospheric correction for shortwave spectral imagery based on MODTRAN4. *Proceedings of SPIE*, **3753**, pp. 61–69.
- BERK, A., ANDERSON, G.P., ACHARYA, P.K., CHETWYND, J.H., HOKE, M.L., BERNSTEIN, L.S., SHETTLE, E.P., MATTHEW, M.W. and ALDER-GOLDEN, S.M., 1999, *MODTRAN4 Version 2 User's Manual*. Air Force Research Laboratory, Space Vehicles Directorate.
- CARMICHAEL, G.R., TANG, Y., KURATA, G., UNO, I., STREETS, D., WOO, J.-H., HUANG, H., YIENGER, J., LEFER, B., SHETTER, R.E., BLAKE, D.R., FRIED, A., APEL, E., EISELE, F., CANTRELL, C., AVERY, M.A., BARRICK, J.D., SACHSE, G.W., BRUNE, W.L., SANDHOLM, S.T., KONDO, Y., SINGH, H.B., TALBOT, R.W., BANDY, A., CLARKE, A.D. and HEIKES, B.G., 2003, Regional-scale chemical transport modeling in support of the analysis of observations obtained during the TRACE-P experiment. *Journal of Geophysical Research*, **108**, p. 8823.
- CARTER, W.P.L., 1999, *Documentation of the SAPRC-99 Chemical Mechanism for VOC Reactivity Assessment*, Contract 92–329, Contract 95–308 (Riverside, CA: California Air Resources Board).
- CLINTON, N.E., POTTER, C., CRABTREE, B., GENOVESE, V., GROSS, P. and GONG, P., 2010, Remote sensing-based time-series analysis of cheatgrass (*Bromus tectorum* L.) phenology. *Journal of Environmental Quality*, **39**, pp. 955–963.
- HOOK, S., MYERS, J.J., THOME, K.J., FITZGERALD, M. and KAHLEA, A.B., 2001, The MODIS/ASTER airborne simulator (MASTER) – a new instrument for earth science studies. *Remote Sensing of Environment*, **76**, pp. 93–102.
- HUANG, H., GONG, P., CLINTON, N. and HUI, F., 2008, Reduction of atmospheric and topographic effect on Landsat TM data for forest classification. *International Journal of Remote Sensing*, **29**, pp. 5623–5642.
- HUANG, M., CARMICHAEL, G.R., ADHIKARY, B., SPAK, S.N., KULKARNI, S., CHENG, Y.F., WEI, C., TANG, Y., PARRISH, D.D., OLTMANS, S.J., D'ALLURA, A., KADUWELA, A., CAI, C., WEINHEIMER, A.J., WONG, M., PIERCE, R.B., AL-SAAFI, J.A., STREETS, D.G. and ZHANG, Q., 2010a, Impacts of transported background ozone on California air quality during the ARCTAS-CARB period—a multi-scale modeling study. *Atmospheric Chemistry & Physics*, **10**, pp. 6947–6968.
- HUANG, M., CARMICHAEL, G.R., SPAK, S.N., ADHIKARY, B., KULKARNI, S., CHENG, Y., WEI, C., TANG, Y., D'ALLURA, A., WENBERG, P., HUEY, G., DIBB, J., JIMENEZ, J.L.,

- WEINHEIMER, A.J., KADUWELA, A., CAI, C., WONG, M., PIERCE, R.B., AL-SAAD, J.A., STREETS, D.G. and ZHANG, Q., 2010b, Multi-scale modeling study of the source contributions to near-surface ozone and sulfur oxides levels over California during the ARCTAS-CARB period. *Atmospheric Chemistry & Physics Discussions*, **10**, doi: 10.5194/acpd-10-2777-2010.
- HUETE, A., DIDAN, K., MIURA, T., RODRIGUEZ, E.P., GAO, X. and FERREIRA, L.G., 2002, Overview of the radiometric and biophysical performance of the MODIS vegetation indices. *Remote Sensing of Environment*, **83**, pp. 195–213.
- LEE, C., MARTIN, R.V., VAN DONKELAAR, A., O'BYRNE, G., KROTKOV, N., RICHTER, A., HUEY, L.G. and HOLLOWAY, J.S., 2009, Retrieval of vertical columns of sulfur dioxide from SCIAMACHY and OMI: air mass factor algorithm development, validation, and error analysis. *Journal of Geophysical Research*, **114**, pp. 1–20.
- LETELIER, R.M. and ABBOTT, M.R., 1996, An analysis of chlorophyll fluorescence algorithms for the moderate resolution imaging spectrometer (MODIS). *Remote Sensing of Environment*, **58**, pp. 215–223.
- LO, C.P., QUATTROCHI, D.A. and LUVAL, J.C., 1997, Application of high-resolution thermal infrared remote sensing and GIS to assess the urban heat island effect. *International Journal of Remote Sensing*, **18**, pp. 287–304.
- MARTIN, R.V., 2002, An improved retrieval of tropospheric nitrogen dioxide from GOME. *Journal of Geophysical Research*, **107**, pp. 4437–4458.
- PALMER, P.I., JACOB, D.J., CHANCE, K., MARTIN, V. and KUROSU, P., 2001, Air mass factor formulation for spectroscopic measurements from satellites: application to formaldehyde retrievals from the Global Ozone Monitoring Experiment. *Journal of Geophysical Research*, **106**, pp. 14539–14550.
- RYAN, J.P., GOWER, J.F.R., KING, S.A., BISSETT, W.P., FISCHER, A.M., KUDELA, R.M., KOLBER, Z., MAZZILLO, F., RIENECKER, E.V. and CHAVEZ, F.P., 2008, A coastal ocean extreme bloom incubator. *Geophysical Research Letters*, **35**, pp. 4–8.
- SCHMUGGE, T., FRENCH, A., RITCHIE, J.C., RANGO, A. and PELGRUM, H., 2002, Temperature and emissivity separation from multispectral thermal infrared observations. *Remote Sensing of Environment*, **79**, pp. 189–198.
- SKAMAROCK, W.C., KLEMP, J.B., DUDHIA, J., GILL, D.O., BARKER, D.M., WANG, W., and POWER, J.G., 2005, *A Description of the Advanced Research WRF Version 2*. Technical Note (Boulder, CO: NCAR).
- TANRE, D., HOLBEN, B.N. and KAUFMAN, Y.J., 1992, Atmospheric correction algorithm for NOM-AVHRR products: theory and application. *IEEE Transactions on Geoscience and Remote Sensing*, **30**, pp. 231–248.
- VERHOEF, W. and BACH, H., 2003, Simulation of hyperspectral and directional radiance images using coupled biophysical and atmospheric radiative transfer models. *Remote Sensing of Environment*, **87**, pp. 23–41.
- VERMOTE, E.F., EL SALEOUS, N., JUSTICE, C.O., KAUFMAN, Y.J., PRIVETTE, J.L., REMER, L., ROGER, J.C. and TANRÉ, D., 1997, Atmospheric correction of visible to middle-infrared EOS-MODIS data over land surfaces: background, operational algorithm and validation. *Journal of Geophysical Research*, **102**, pp. 17131–17141.